C. R. Mecanique 343 (2015) 38–56

Contents lists available at ScienceDirect

Comptes Rendus Mecanique

www.sciencedirect.com

Entropy generation in a variable viscosity channel flow of nanofluids with convective cooling

Michael Hamza Mkwizu [a,*], Oluwole Daniel Makinde [b]

[a] Computation and Communication Science and Engineering, Nelson Mandela African Institution of Science and Technology (NM-AIST), P.O. Box 447, Arusha, Tanzania
[b] Faculty of Military Science, Stellenbosch University, Private Bag X2, Saldanha 7395, South Africa

ARTICLE INFO

Article history:
Received 15 April 2014
Accepted 4 September 2014
Available online 3 October 2014

Keywords:
Channel flows
Nanofluids
Variable viscosity
Entropy generation
Bejan number

ABSTRACT

The present work investigates the combined effects of thermophoresis, Brownian motion and variable viscosity on entropy generation in an unsteady flow of water-based nanofluids confined between two parallel plates with convective heat exchange with the ambient surrounding at the walls. Both first and second laws of thermodynamics are applied to analyse the problem. The nonlinear governing equations of continuity, momentum, energy, and nanoparticles concentration are tackled numerically using a semi-discretisation finite-difference method together with a Runge–Kutta–Fehlberg integration scheme. Numerical results for velocity, temperature, and nanoparticles concentration profiles are obtained and utilised to compute the skin friction, the Nusselt number, the entropy generation rate, the irreversibility ratio, and the Bejan number. Pertinent results are displayed graphically and discussed quantitatively.

1. Introduction

Heat-transfer enhancement in engineering and industrial systems is one of the hottest topics in research today. With the growing demand for efficient cooling systems, more effective coolants are required to keep the temperature of heat-generating engines and engineering devices such as electronic components below safe limits. In recent time, the use of nanofluids has provided an innovative technique to enhance heat transfer. Nanotechnology has been widely used in engineering and industry, since nanometer-sized materials possess unique physical and chemical properties. The addition of nanoscale particles into the conventional fluids like water, engine oil, ethylene glycol, etc., is known as nanofluid and was firstly introduced by Choi [1]. Moreover, the effective thermal conductivity of conventional fluids increases remarkably with the addition of metallic nanoparticles with high thermal conductivity. Nanofluids may be considered as single phase flows in low solid concentration because of very small sized solid particles. There are many experimental and theoretical studies on the flow of nanofluids in different geometries [2–9]. A numerical study of buoyancy-driven flow and heat transfer of an alumina (Al_2O_3)–water-based nanofluid in a rectangular cavity was done by Hwang et al. [10]. The nanofluid in the enclosure was assumed to be in a single phase. It was found that for any given Grashof number, the average Nusselt number increased with the solid volume concentration parameter. Nield and Kuznetsov [11] investigated numerically the Cheng–Minkowycz problem for a natural convective boundary-layer flow in a porous medium saturated by a nanofluid. Oztop and Abu-Nada [12] considered natural convection in partially heated enclosures having different aspect ratios and filled with a nanofluid. They found that the heat transfer was more pronounced at low aspect ratios and high volume fractions of nanoparticles.

* Corresponding author.
E-mail addresses: mkwizumh@gmail.com, mkwizum@nm-aist.ac.tz (M.H. Mkwizu), makinded@gmail.com (O.D. Makinde).

http://dx.doi.org/10.1016/j.crme.2014.09.002
1631-0721/

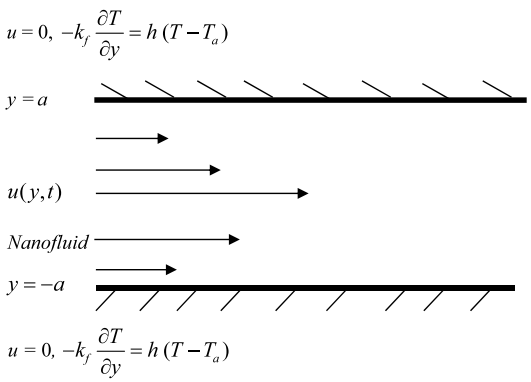

Fig. 1. (Colour online.) Schematic diagram of the problem under consideration.

Ibrahim and Makinde [13] studied the effect of double stratification on the boundary-layer flow and the heat transfer of nanofluid over a vertical plate. The buoyancy effects on the stagnation point flow and heat transfer of a nanofluid past a convectively heated stretching/shrinking sheet with or without magnetic field were considered by Makinde et al. [14] and Makinde [15]. Wang and Mujumdar [16] presented a comprehensive review of heat transfer characteristics of nanofluids. Detailed reports on convective transport in nanofluids can be found in Buongiorno [17], Mutuku-Njane and Makinde [18], Tiwari and Das [19], etc.

Meanwhile, in the nanofluids flows, the improvement of the heat transfer properties causes a reduction in entropy generation. The foundation of knowledge of entropy production goes back to Clausius and Kelvin's studies on the irreversible aspects of the second law of thermodynamics. Since then the theories based on these foundations have rapidly developed, see Bejan [20,21]. However, the entropy production resulting from heat and mass transfer coupled with viscous dissipation in nanofluids has remained untreated by classical thermodynamics, which motivates many researchers to conduct analyses of fundamental and applied engineering problems based on second law analysis with respect to nanofluid. Based on the concept of efficient energy use and the minimal entropy generation principle, optimal designs of thermodynamic systems have been widely proposed base on the second law of thermodynamics [22]. It is possible to improve the efficiency and overall performance of all kinds of flows and thermal systems through entropy minimisation techniques. The analysis of energy utilisation and entropy generation has become one of the primary objectives in designing a thermal system. This has become the main concern in many fields such as heat exchangers, turbo machinery, electronic cooling, porous media and combustion. Several studies have thoroughly dealt with conventional fluid flow irreversibility due to viscous effect and heat transfer by conduction [23–26]. Makinde et al. [27] performed numerous investigations to calculate entropy production and irreversibility due to flow and heat transfer of nanofluids over a moving flat surface. They found that the entropy generation in the flow system can be minimised by appropriate combination of parameter values together with nanoparticles volume fraction.

In the present study, we analyse the combined effects of thermophoresis, Brownian motion, and variable viscosity on the entropy generation rate in an unsteady channel flow of water-based nanofluid under the influence of convective heat exchange with the ambient surroundings. Such flows are very important in engine cooling, solar water heating, cooling of electronics, cooling of transformer oil, improving diesel generator efficiency, cooling of heat exchanging devices, improving heat-transfer efficiency of chillers, domestic refrigerator and freezers, cooling in machining and in nuclear reactor. In the following sections, the problem is formulated, numerically analysed, and solved. Pertinent results are displayed graphically and discussed.

2. Mathematical model

Consider the unsteady flow of an incompressible variable viscosity nanofluid in a channel between two parallel plates under the combined action of a constant pressure gradient and convective heat exchange with the ambient surrounding. It is assumed that the channel width is $2a$ and the flow is symmetrical with no slip at the walls as depicted in Fig. 1.

$$u = 0, \qquad -k_{\mathrm{f}} \frac{\partial T}{\partial y} = h(T - T_{\mathrm{a}})$$

Using the Buongiorno nanofluid model [17] with the Brownian motion, thermophoresis and nanoparticle volume fraction distributions, the governing equations for continuity, momentum, energy and nanoparticle concentration are:

$$\frac{\partial u}{\partial x} = 0 \tag{1}$$

$$\rho_{\mathrm{f}} \frac{\partial u}{\partial \bar{t}} = -\frac{\partial P}{\partial x} + \frac{\partial}{\partial y}\left(\mu_f(T) \frac{\partial u}{\partial y}\right) \tag{2}$$

$$\frac{\partial T}{\partial \bar{t}} = \alpha_{\mathrm{f}} \frac{\partial^2 T}{\partial y^2} + \tau \left\{ D_{\mathrm{B}} \frac{\partial T}{\partial y} \frac{\partial \phi}{\partial y} + \frac{D_{\mathrm{T}}}{T_{\mathrm{a}}} \left(\frac{\partial T}{\partial y} \right)^2 \right\} + \frac{\alpha_{\mathrm{f}} \mu_{\mathrm{f}}(T)}{k_{\mathrm{f}}} \left(\frac{\partial u}{\partial y} \right)^2 \tag{3}$$

$$\frac{\partial \phi}{\partial \bar{t}} = D_{\mathrm{B}} \frac{\partial^2 \phi}{\partial y^2} + \left(\frac{D_{\mathrm{T}}}{T_{\mathrm{a}}} \right) \left(\frac{\partial^2 T}{\partial y^2} \right) \tag{4}$$

where D_{B} and D_{T} are the Brownian and thermophoretic diffusion coefficients respectively, u is the nanofluid velocity in the x-direction, T is the temperature of the nanofluid, P is the nanofluid pressure, $\bar{t}$ is the time, T_{a} is the ambient temperature, which also correspond to the nanofluid initial temperature, ϕ is the concentration of nanoparticles, ρ_{f} is the density of the nanofluid, μ_{f} is the viscosity of the fluid fraction, α_{f} is the thermal diffusivity of the nanofluid, k_{f} is the thermal conductivity of the fluid fraction and τ is the ratio of the heat capacitance of solid particles to that of the nanofluid. The dynamic viscosity of the nanofluid is assumed to be temperature dependent, as follows:

$$\mu_{\mathrm{f}}(T) = \mu_0 \, \mathrm{e}^{-m(T - T_{\mathrm{a}})} \tag{5}$$

where μ_0 is the nanofluid viscosity at the ambient temperature T_{a}, m is a viscosity variation parameter, which depends on the particular fluid. The initial and boundary conditions are given as follows:

$$u(y,0) = 0, \qquad T(y,0) = T_{\mathrm{a}}, \qquad \phi(y,0) = \phi_0 \tag{6}$$

$$\frac{\partial u}{\partial y}(0,\bar{t}) = \frac{\partial T}{\partial y}(0,\bar{t}) = \frac{\partial \phi}{\partial y}(0,\bar{t}) \quad \text{(axial-symmetric conditions)} \tag{7}$$

$$u(a,\bar{t}) = 0, \qquad -k_{\mathrm{f}} \frac{\partial T}{\partial y}(a,\bar{t}) = h\big(T(a,\bar{t}) - T_{\mathrm{a}}\big), \qquad D_{\mathrm{B}} \frac{\partial \phi}{\partial y}(a,\bar{t}) = -\frac{D_{\mathrm{T}}}{T_{\mathrm{a}}} \frac{\partial T}{\partial y}(a,\bar{t}) \tag{8}$$

where h is the heat transfer coefficient and ϕ_0 is the nanoparticles initial concentration. We introduce the non-dimensionless variables and parameters as follows:

$$\left.\begin{aligned}
&\theta = \frac{T - T_{\mathrm{a}}}{T_{\mathrm{a}}}, \qquad W = \frac{ua}{\upsilon_{\mathrm{f}}}, \qquad \eta = \frac{y}{a}, \qquad t = \frac{\bar{t}\upsilon_f}{a^2}, \qquad \upsilon_{\mathrm{f}} = \frac{\mu_0}{\rho_{\mathrm{f}}}, \qquad Bi = \frac{ha}{k_{\mathrm{f}}} \\
&\overline{P} = \frac{a^2 P}{\mu_0^2}, \qquad Nb = \frac{\tau D_B \phi_0}{\alpha_f}, \qquad A = -\frac{\partial \overline{P}}{\partial X}, \qquad X = \frac{x}{a}, \qquad Pr = \frac{\mu_0 c_{\mathrm{pf}}}{k_{\mathrm{f}}}, \qquad Sc = \frac{\upsilon_{\mathrm{f}}}{D_{\mathrm{B}}} \\
&Ec = \frac{\upsilon_f^2}{c_{\mathrm{pf}} T_{\mathrm{a}} a^2}, \qquad H = \frac{\phi}{\phi_0}, \qquad Nt = \frac{\tau D_{\mathrm{T}}}{\alpha_{\mathrm{f}}}, \qquad \tau = \frac{(\rho c_{\mathrm{p}})_{\mathrm{s}}}{(\rho c_{\mathrm{p}})_{\mathrm{f}}}, \qquad \beta = m T_{\mathrm{a}}
\end{aligned}\right\} \tag{9}$$

The dimensionless governing equations together with the appropriate initial and boundary conditions can be written as:

$$\frac{\partial W}{\partial t} = A + \mathrm{e}^{-\beta\theta} \frac{\partial^2 W}{\partial \eta^2} - \beta \, \mathrm{e}^{-\beta\theta} \frac{\partial \theta}{\partial \eta} \frac{\partial W}{\partial \eta} \tag{10}$$

$$Pr \frac{\partial \theta}{\partial t} = \frac{\partial^2 \theta}{\partial \eta^2} + \left\{ Nb \frac{\partial \theta}{\partial \eta} \frac{\partial H}{\partial \eta} + Nt \left(\frac{\partial \theta}{\partial \eta} \right)^2 \right\} + Ec \, Pr \, \mathrm{e}^{-\beta\theta} \left(\frac{\partial W}{\partial \eta} \right)^2 \tag{11}$$

$$Sc \frac{\partial H}{\partial t} = \frac{\partial^2 H}{\partial \eta^2} + \frac{Nt}{Nb} \frac{\partial^2 \theta}{\partial \eta^2} \tag{12}$$

with

$$W(\eta,0) = 0, \qquad \theta(\eta,0) = 0, \qquad H(\eta,0) = 1 \tag{13}$$

$$\frac{\partial W}{\partial \eta}(0,t) = \frac{\partial \theta}{\partial \eta}(0,t) = \frac{\partial H}{\partial \eta}(0,t) = 0 \tag{14}$$

$$W(1,t) = 0, \qquad \frac{\partial \theta}{\partial \eta}(1,t) = -Bi\theta(1,t), \qquad \frac{\partial H}{\partial \eta}(1,t) = -\frac{Nt}{Nb} \frac{\partial \theta}{\partial \eta}(1,t) \tag{15}$$

where Nb is the Brownian motion parameter, Bi is the Biot number, Nt is the thermophoresis parameter, Sc is the Schmidt number, Pr is the Prandtl number, Ec is the Eckert number and A is the pressure gradient parameter. The quantities of practical interest in this study are the skin friction coefficient C_{f} and the local Nusselt number Nu, which are defined as

$$C_f = \frac{a^2 \tau_w}{\rho_f \upsilon_f^2}, \qquad Nu = \frac{a q_w}{k_f T_a} \tag{16}$$

where τ_w is the wall shear stress and q_w is the heat flux at the channel walls given by

$$\tau_w = \mu_f \frac{\partial u}{\partial y}\bigg|_{y=a}, \qquad q_w = -k_f \frac{\partial T}{\partial y}\bigg|_{y=a} \tag{17}$$

Substituting Eqs. (17) into (16), we obtain:

$$\left.\begin{aligned} C_f &= e^{-\beta\theta} \frac{\partial W}{\partial \eta} \\ Nu &= -\frac{\partial \theta}{\partial \eta} \end{aligned}\right\} \quad \text{at } \eta = 1 \tag{18}$$

3. Entropy analysis

In the nanofluids flows, the improvement of the heat transfer properties causes a reduction in entropy generation. However, a convection process involving a channel flow of nanofluids is inherently irreversible. The non-equilibrium conditions due to the exchange of energy and momentum, within the nanofluid and at solid boundaries, cause continuous entropy generation [20,21]. One part of this entropy production results from heat transfer in the direction of finite temperature gradients, while another part arises due to the fluid friction, nanoparticle concentration and complex interaction between the base fluid and the nanoparticles. According to Woods [22], the local volumetric rate of entropy generation is given by:

$$S''' = \frac{k_f}{T_a^2}\left(\frac{\partial T}{\partial y}\right)^2 + \frac{\mu_f(T)}{T_a}\left(\frac{\partial u}{\partial y}\right)^2 + \frac{D_B}{\phi_0}\left(\frac{\partial \phi}{\partial y}\right)^2 + \frac{D_B}{T_a}\frac{\partial T}{\partial y}\frac{\partial \phi}{\partial y} \tag{19}$$

The first term in Eq. (19) is the irreversibility due to heat transfer; the second term is the entropy generation due to viscous dissipation, while the third and the fourth terms are the local entropy generation due to mass transfer of the nanoparticles and their complex interaction with the base fluid. Using Eq. (9), we express the entropy generation number in dimensionless form as

$$Ns = \frac{a^2 S'''}{k_f} = \left(\frac{\partial \theta}{\partial \eta}\right)^2 + Br\, e^{-\beta\theta}\left(\frac{\partial W}{\partial \eta}\right)^2 + \lambda\left[\left(\frac{\partial H}{\partial \eta}\right)^2 + \frac{\partial H}{\partial \eta}\frac{\partial \theta}{\partial \eta}\right] \tag{20}$$

where $Br = Ec\,Pr$ is the Brinkmann number, $\lambda = \phi_0 D_B / k_f$ is the nanoparticles mass transfer parameter. Let

$$N_1 = \left(\frac{\partial \theta}{\partial \eta}\right)^2, \qquad N_2 = Br\, e^{-\beta\theta}\left(\frac{\partial W}{\partial \eta}\right)^2, \qquad N_3 = \lambda\left[\left(\frac{\partial H}{\partial \eta}\right)^2 + \frac{\partial H}{\partial \eta}\frac{\partial \theta}{\partial \eta}\right] \tag{21}$$

The irreversibility distribution ratio is defined as $\Phi = N_2/(N_1 + N_3)$. Heat and nanoparticles mass transfer irreversibility dominates for $0 \le \Phi < 1$ and fluid friction irreversibility dominates when $\Phi > 1$. The contributions of both irreversibilities to entropy generation are equal when $\Phi = 1$. We define the Bejan numbers (Be) mathematically as

$$Be = \frac{N_1 + N_3}{Ns} = \frac{1}{1 + \Phi} \tag{22}$$

From Eq. (22), it is very obvious that the Bejan number ranges from 0 to 1. The zero value of the Bejan number corresponds to the limit where the irreversibility is dominated by the effect of fluid friction, while $Be = 1$ is the limit where the irreversibility due to heat and nanoparticles mass transfer dominates the flow system. Heat and mass transfer, together with fluid friction irreversibilities, are the same when the Bejan number equals 0.5.

4. Numerical procedure

Eqs. (10)–(15) constitute a system of nonlinear initial boundary value problems (IBVPs) and are solved numerically using a semi-discretisation finite-difference method known as method of lines. A partition of the spatial interval $0 \le \eta \le 1$ into N equal parts is introduced such that the grid size $\Delta\eta = 1/N$ and grid points $\eta_i = (i-1)\Delta\eta$, $1 \le i \le N+1$. The semi-discretisation finite difference technique known as method of line [28] is employed to tackle the model nonlinear initial boundary value problem in (10)–(15). The discretisation is based on a linear Cartesian mesh and a uniform grid on which finite differences are taken. The first and second spatial derivatives in Eqs. (10)–(12) are approximated with second-order central finite differences. Let $W_i(t)$, $\theta_i(t)$ and $H_i(t)$ be approximation of $W(\eta_i, t)$, $\theta(\eta_i, t)$ and $H(\eta_i, t)$, then the semi-discrete system for the problem becomes

$$\frac{dW_i}{dt} = A + e^{-\beta\theta_i}\frac{(W_{i+1} - 2W_i + W_{i-1})}{(\Delta\eta)^2} - \beta\, e^{-\beta\theta_i}\frac{(\theta_{i+1} - \theta_{i-1})(W_{i+1} - W_{i-1})}{4(\Delta\eta)^2} \tag{23}$$

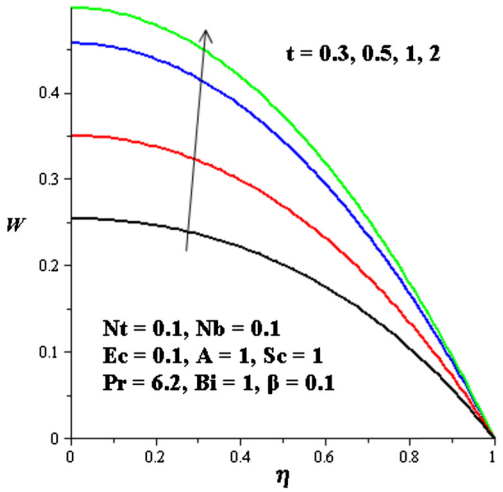

Fig. 2. (Colour online.) Velocity profiles across the channel with increasing time.

$$Pr\frac{\mathrm{d}\theta_i}{\mathrm{d}t} = \frac{(\theta_{i+1} - 2\theta_i + \theta_{i-1})}{(\Delta\eta)^2} + Nb\frac{(\theta_{i+1} - \theta_{i-1})(H_{i+1} - H_{i-1})}{4(\Delta\eta)^2} + Nt\left(\frac{\theta_{i+1} - \theta_{i-1}}{2\Delta\eta}\right)^2 + Ec\,Pr\,\mathrm{e}^{-\beta\theta_i}\left(\frac{W_{i+1} - W_{i-1}}{2\Delta\eta}\right)^2 \tag{24}$$

$$Sc\frac{\mathrm{d}H_i}{\mathrm{d}t} = \frac{(H_{i+1} - 2H_i + H_{i-1})}{(\Delta\eta)^2} + \frac{Nt}{Nb}\frac{(\theta_{i+1} - 2\theta_i + \theta_{i-1})}{(\Delta\eta)^2} \tag{25}$$

with initial conditions

$$W_i(0) = \theta_i(0) = 0, \qquad H_i(0) = 1, \quad 1 \le i \le N+1 \tag{26}$$

The equations corresponding to the first and last grid points are modified to incorporate the boundary conditions, as follows:

$$W_2 = W_1, \qquad \theta_2 = \theta_1, \qquad H_2 = H_1, \qquad w_{N+1} = 0$$
$$\theta_{N+1} = \theta_N(1 - Bi\Delta\eta), \qquad H_{N+1} = H_N - Nt\frac{(\theta_{N+1} - \theta_N)}{Nb} \tag{27}$$

There is only one independent variable in Eqs. (23)–(26), so they are first-order ordinary differential equations with known initial conditions. The resulting initial value problem can be easily solved iteratively using the Runge–Kutta–Fehlberg integration technique [28] implemented on computer using Matlab. From the process of numerical computation, the skin-friction coefficient and the Nusselt number in Eq. (18) are also worked out and their numerical values are presented.

5. Results and discussion

Numerical solution for the representative velocity field, temperature field, nanoparticles concentration, skin friction, Nusselt number, entropy generation rate and Bejan number have been carried out by assigning some arbitrary chosen specific values to various thermophysical parameters controlling the flow system (see Figs. 2–35). Following Hwang et al. [10], the Prandtl number (Pr) of the pure water-based nanofluid under consideration is assigned the value 6.2.

5.1. Effects of parameter variations on velocity profiles

Figs. 2–6 depict the effects of various physical parameters on the nanofluid velocity profiles. Generally, the velocity profile is maximum along the channel centreline and minimum at the walls. This can be attributed to the strong boundary layer effects at the walls due to the nanofluid viscosity and the impose no-slip condition at the walls. It can be noted in Figs. 2–3 that as time t increases, the velocity increases across the channel until it attains a steady-state profile for a given set of parameter values. Fig. 4 shows that the nanofluid velocity profile decreases with increasing convective cooling at the walls as the Biot number Bi increases. This may be attributed to an increase of the rate of heat loss at the channel walls, leading to an increase in the nanofluid thickness and a decrease in the flow speed. In Fig. 5, we observed that the velocity of the nanofluid increases with a decrease in viscosity due to a temperature increase. This is expected, since, as β increases, the

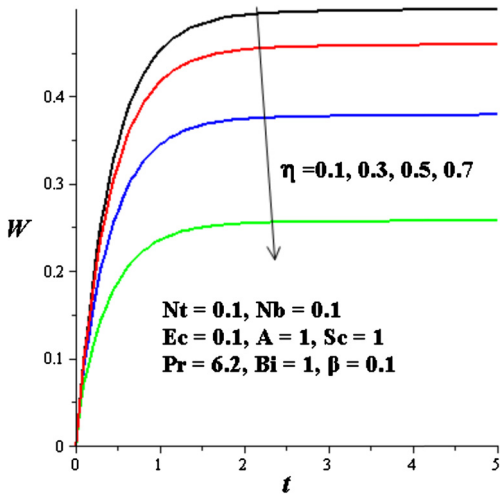

Fig. 3. (Colour online.) Velocity profiles across the channel with increasing time.

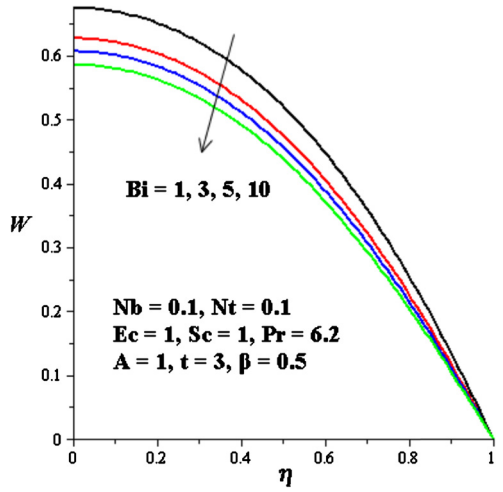

Fig. 4. (Colour online.) Velocity profiles with increasing *Bi*.

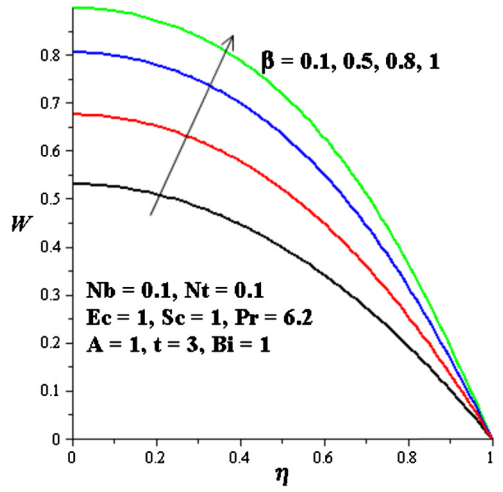

Fig. 5. (Colour online.) Velocity profiles with increasing β.

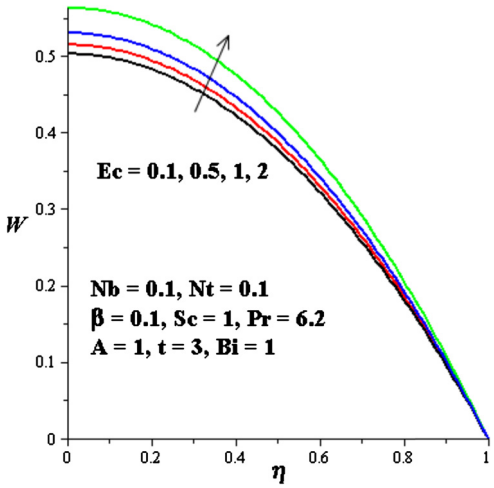

Fig. 6. (Colour online.) Velocity profiles with increasing *Ec*.

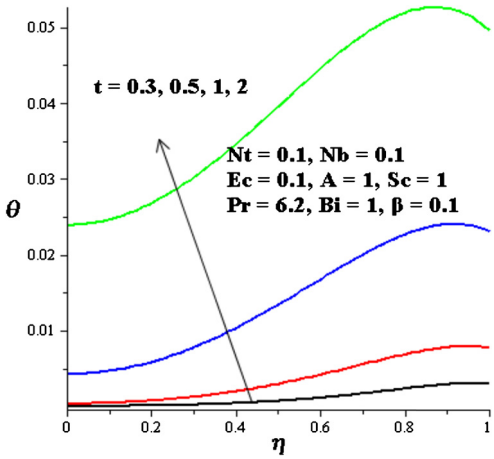

Fig. 7. (Colour online.) Temperature profiles with increasing time.

fluid's viscosity decreases due a temperature rise; consequently, the fluid becomes lighter and flow faster. A similar trend is observed in Fig. 6, with an increase of the Eckert number *Ec* due to viscous dissipation. The nanofluid kinetic energy increases with viscous heating; this invariably leads to a decrease in the fluid viscosity and an increase in the velocity profile.

5.2. Effects of parameter variations on temperature profiles

Figs. 7–11 illustrate the effects of unsteadiness and parameter variation on the temperature profiles. In Figs. 7–8, we observed the nanofluid temperature increases across the channel with time and space. However, the temperature tends to be lower within the channel centreline region. Fig. 9 shows that the fluid temperature decreases across the channel with increasing convective cooling due to increasing heat loss toward the ambient surrounding from the walls. As β increases, the nanofluid viscosity decreases; consequently, the kinetic energy of nanoparticles increase and a rise in nanofluid temperature is observed, as shown in Fig. 10. A similar trend is noticed with increasing *Ec* in Fig. 11: the temperature of the nanofluid increases due to an increase in the viscous heating effect.

5.3. Effects of parameter variations on nanoparticles concentration

Figs. 12–18 depict the effects of various physical parameters on the nanoparticles concentration profile. It is observed that the concentration of nanoparticles increases along the channel centreline region $0 \leq \eta \leq 0.5$ and decreases near the walls as time increases, as shown in Figs. 12–13. Fig. 14 shows that nanoparticle concentration decreases within the centreline region, whereas it increases near the walls as *Bi* increases. This may be attributed to the fact that the kinetic energy of the nanoparticles increases towards the wall with a rise in convective heat loss to the ambient. In Figs. 15–16, a rise in

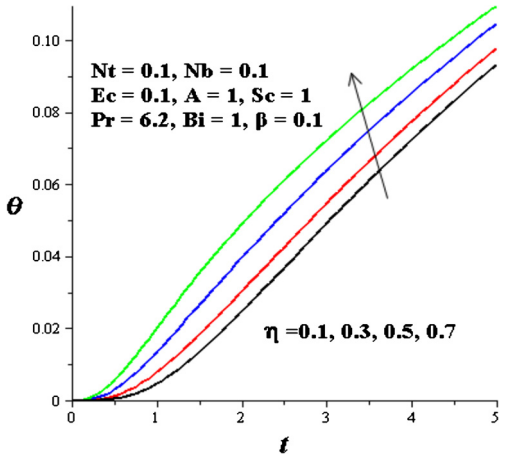

Fig. 8. (Colour online.) Temperature profiles with increasing time.

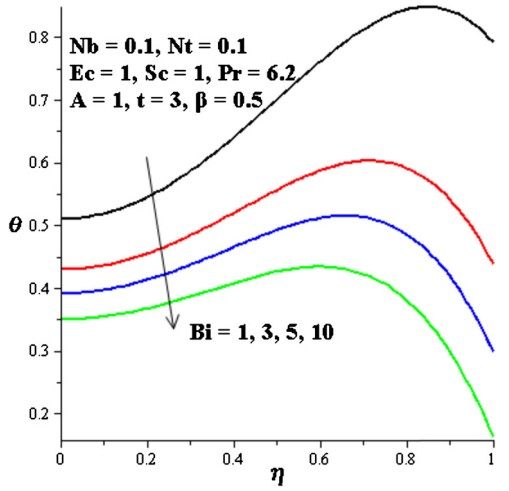

Fig. 9. (Colour online.) Temperature profiles with increasing *Bi*.

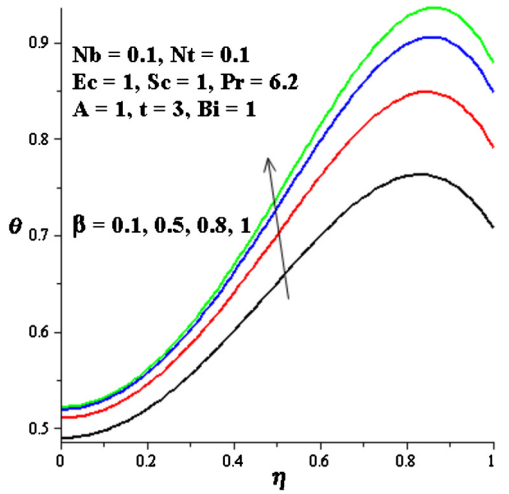

Fig. 10. (Colour online.) Temperature profiles with increasing β.

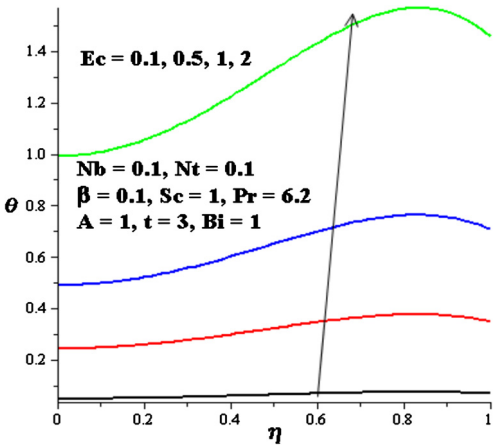

Fig. 11. (Colour online.) Temperature profiles with increasing *Ec*.

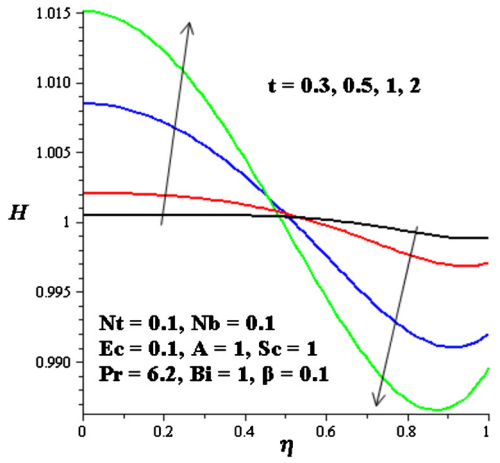

Fig. 12. (Colour online.) Nanoparticle distribution with increasing time.

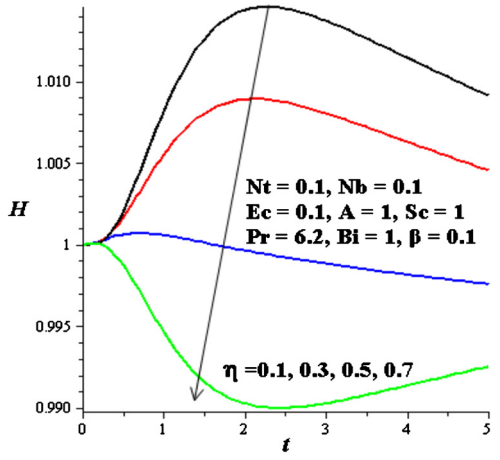

Fig. 13. (Colour online.) Nanoparticle distribution with increasing time.

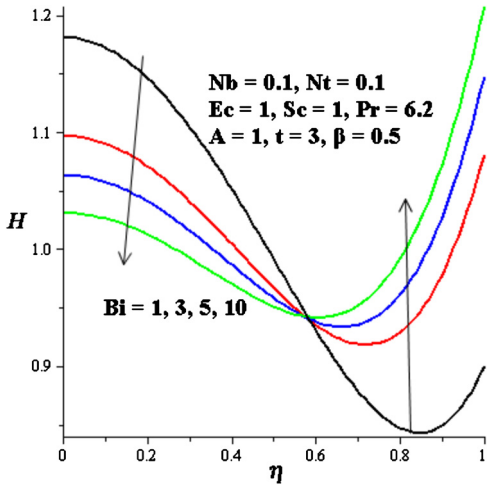

Fig. 14. (Colour online.) Nanoparticle distribution with increasing *Bi*.

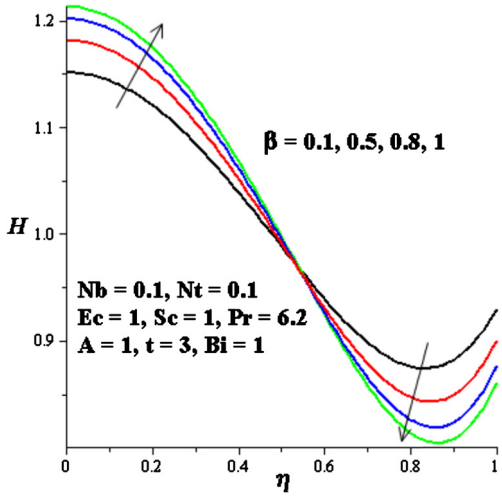

Fig. 15. (Colour online.) Nanoparticle distribution with increasing β.

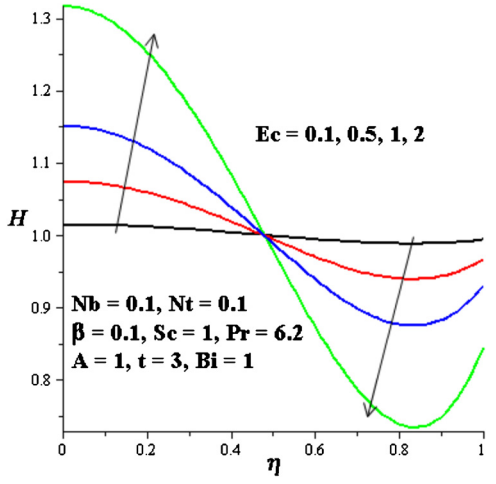

Fig. 16. (Colour online.) Nanoparticle distribution with increasing *Ec*.

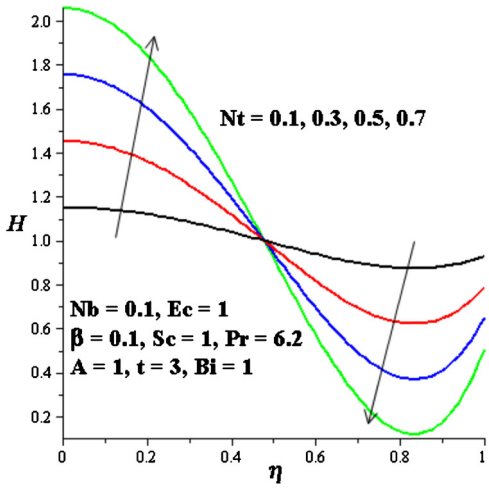

Fig. 17. (Colour online.) Nanoparticle distribution with increasing *Nt*.

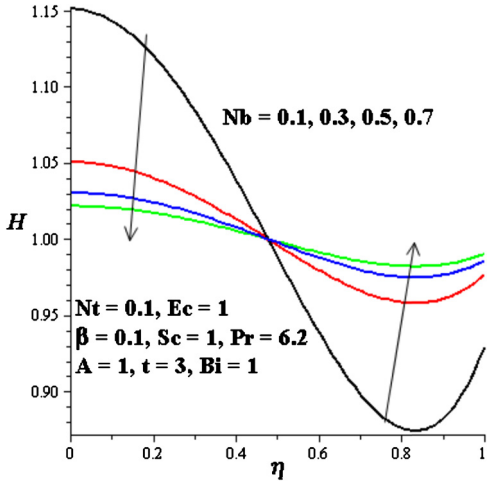

Fig. 18. (Colour online.) Nanoparticle distribution with increasing *Nb*.

nanoparticles concentration towards the channel centreline region is observed, with an increase in β and *Ec*. Interestingly, as β and *Ec* increase, the viscosity of the nanofluid decreases while the temperature and velocity increase towards the channel centreline; consequently, nanoparticle concentration increases along the centreline region and decreases near the walls. A similar trend is observed in Fig. 17, with an increasing thermophoresis effect *Nt* due to the temperature gradient, leading to an increase in nanoparticle concentration towards the channel centreline region. Moreover, an increasing motion of particles (Brownian motion *Nb*) in a fluid, as shown in Fig. 18, may cause a decrease in nanoparticle concentration within the centreline region and an increase near the walls.

5.4. Effects of parameter variations on skin friction and the Nusselt number

Table 1 shows the effect of parameter variation on skin friction. It can be seen that skin friction at the channel walls increases with time and when increasing the values of *Bi*, β, *Nb*, and *A*. This may be attributed to a rise in the velocity gradient at the walls due to combined effects of convective cooling, viscosity variation, Brownian motion and pressure gradient. Meanwhile, a decrease in skin friction is observed with increasing parameter values of *Ec* and *Nt*. In Fig. 19, we observed a rise in the heat flux at the walls with time and when increasing the values of *Ec*, *Bi*, and β. It is evidenced that a decrease in fluid viscosity, coupled with the combined increase in viscous heating and convective cooling, increases the temperature gradient at the channel walls; consequently, the Nusselt number increases.

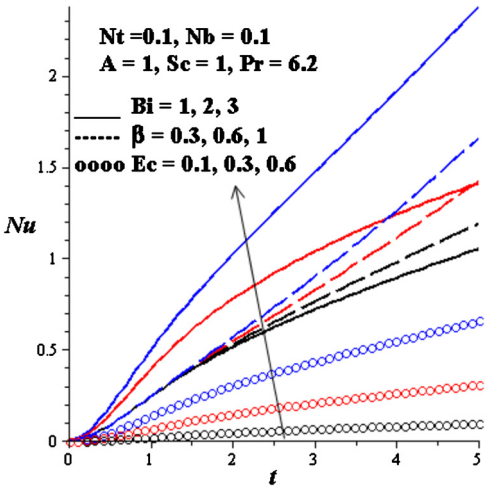

Fig. 19. (Colour online.) Nusselt number profiles.

Table 1
Computation showing the skin friction $Pr = 6.2$, $Sc = 1$.

T	Bi	β	Ec	Nt	Nb	A	C_f
1.0	1.0	0.1	0.1	0.1	0.1	1.0	1.087385958
3.0	1.0	0.1	0.1	0.1	0.1	1.0	1.097675134
5.0	1.0	0.1	0.1	0.1	0.1	1.0	1.109142224
3.0	3.0	0.1	0.1	0.1	0.1	1.0	1.113883200
3.0	5.0	0.1	0.1	0.1	0.1	1.0	1.120076893
3.0	1.0	0.5	0.1	0.1	0.1	1.0	1.656399435
3.0	1.0	1.0	0.1	0.1	0.1	1.0	2.854667188
3.0	1.0	0.1	0.5	0.1	0.1	1.0	1.070051922
3.0	1.0	0.1	1.0	0.1	0.1	1.0	1.032125297
3.0	1.0	0.1	0.1	0.3	0.1	1.0	1.083224047
3.0	1.0	0.1	0.1	0.5	0.1	1.0	1.068774187
3.0	1.0	0.1	0.1	0.1	0.3	1.0	1.102492475
3.0	1.0	0.1	0.1	0.1	0.5	1.0	1.103455943
3.0	1.0	0.1	0.1	0.1	0.1	2.0	1.192432794
3.0	1.0	0.1	0.1	0.1	0.1	3.0	1.282885825

5.5. Effects of parameter variations on the entropy generation rate

Figs. 20–26 illustrate the effect of parameter variation on the entropy generation rate across the channel. From Figs. 20–21, it can be seen that the entropy generation rate increases with time and is minimum along the channel centreline and maximum at the walls. This may be attributed to the fact that entropy production depends on velocity, temperature and nanoparticle concentration gradients, which vanish along the channel centreline, leading to a minimum entropy generation within this region. Moreover, an increase in the Biot number decreases entropy generation within the channel, but increases entropy generation at the walls, as shown in Fig. 22. In Figs. 23–24, we observe a general increase in entropy production across the channel with increasing viscous heating and a decrease in nanofluid viscosity. A similar trend is observed in Fig. 25 with increasing entropy production as the pressure gradient increases. This is because mixtures of nanoparticles in the fluid with different responses to the pressure gradient increase the velocity gradient; consequently, the entropy generation rate increases. Fig. 26 shows that an increase in the thermophoresis effect due to temperature gradient increases the entropy generation rate within the channel and at the walls.

5.6. Effects of parameter variations on the Bejan number

The variation in the Bejan number with time and the transverse distance is shown in Figs. 27–35 for different parameters. In Figs. 27–28, one can observe that the Bejan number increases with time within the channel and at the walls. Moreover, a maximum value of the Bejan number is noticed along the channel centreline region as compared to the walls. Clearly, increasing the Bejan number provokes a rise in the dominant effects of heat transfer and an irreversibility of the mass transfer of the nanoparticles along the centreline region and at the walls. It is noteworthy that a region very close to the walls exists where the Bejan number is zero and the irreversibility is dominated by the fluid friction. Fig. 29 shows that the Bejan number decreases along the centreline region and increases near the walls, with a rise in convective cooling; consequently, the dominant effect of fluid friction irreversibility increases along the centreline region, while the heat and

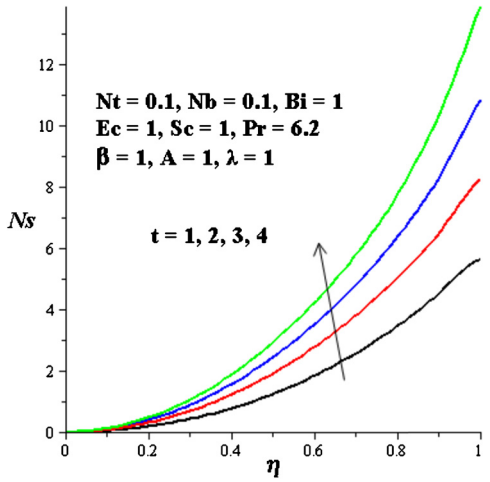

Fig. 20. (Colour online.) Entropy generation with increasing time.

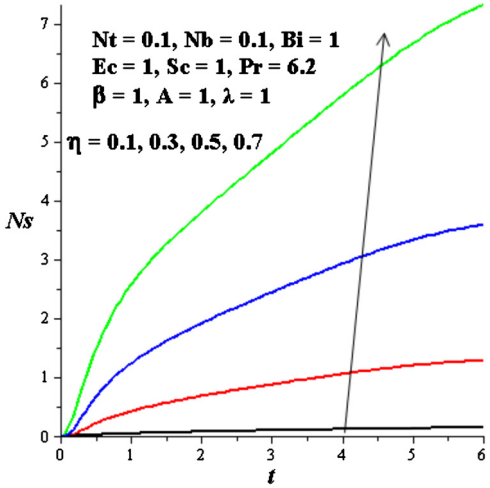

Fig. 21. (Colour online.) Entropy generation with increasing time.

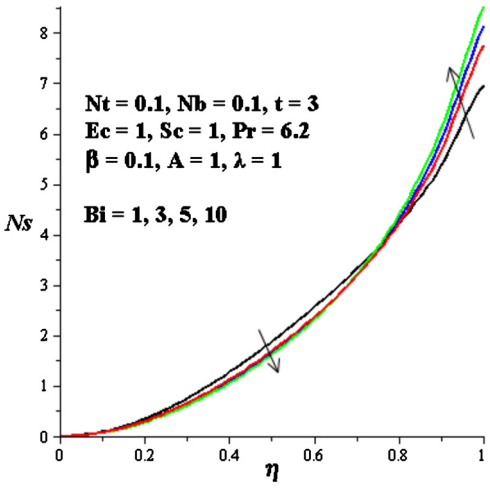

Fig. 22. (Colour online.) Entropy generation with increasing *Bi*.

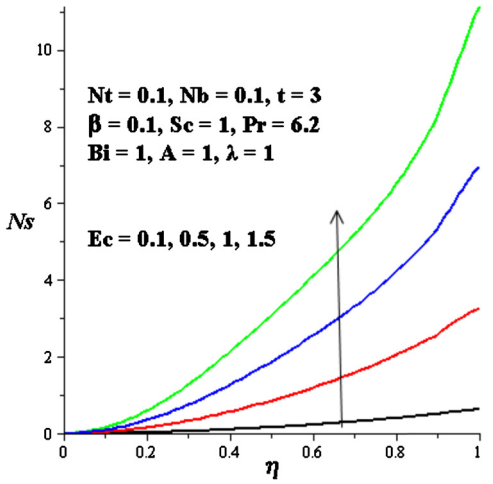

Fig. 23. (Colour online.) Entropy generation with increasing *Ec*.

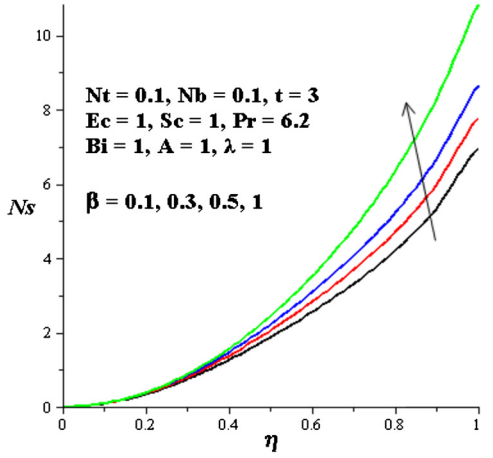

Fig. 24. (Colour online.) Entropy generation with increasing β.

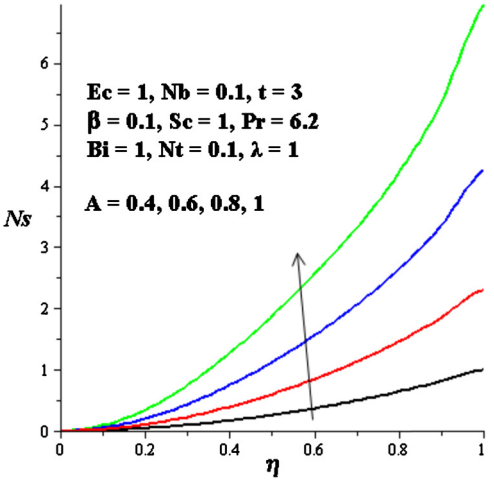

Fig. 25. (Colour online.) Entropy generation with increasing *A*.

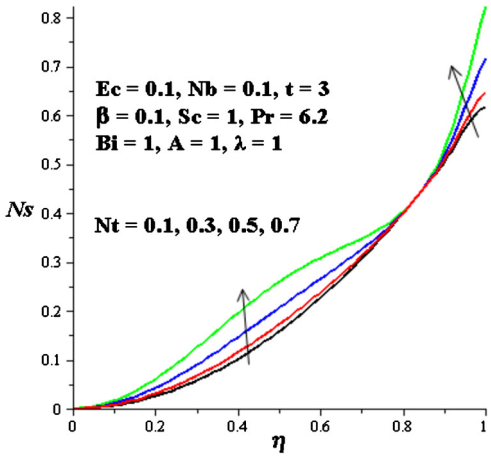

Fig. 26. (Colour online.) Entropy generation with increasing *Nt*.

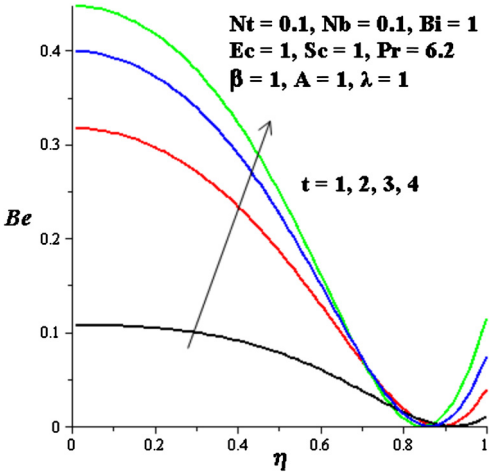

Fig. 27. (Colour online.) Bejan number with increasing time.

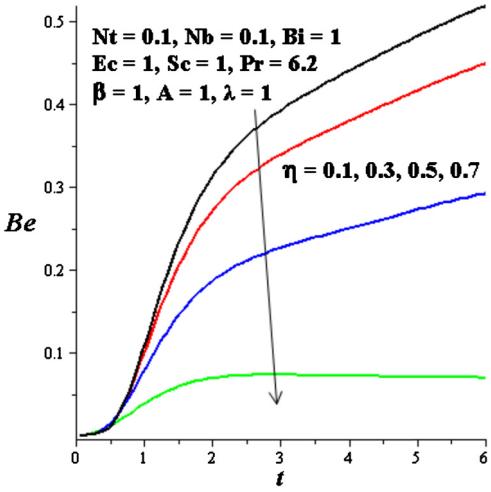

Fig. 28. (Colour online.) Bejan number with increasing time.

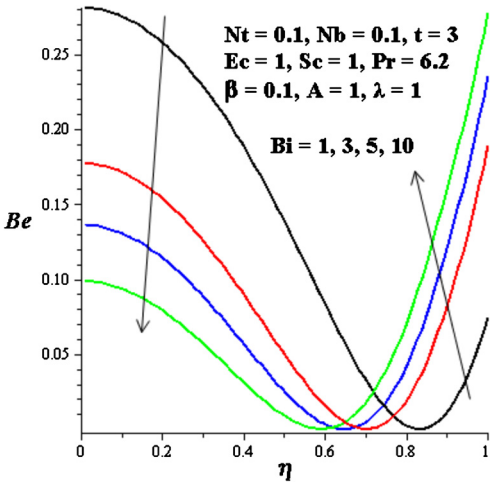

Fig. 29. (Colour online.) Bejan number with increasing *Bi*.

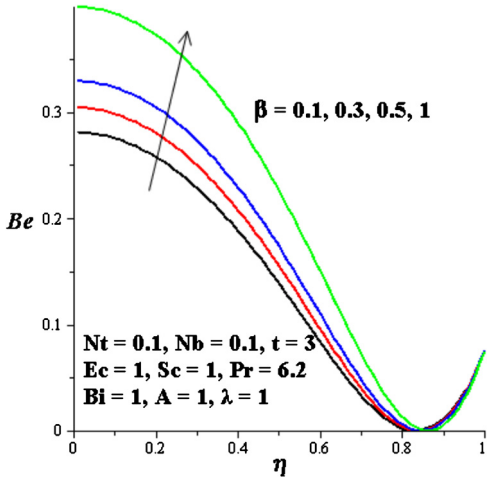

Fig. 30. (Colour online.) Bejan number with increasing β.

mass transfer irreversibilities effect dominates along the walls. In Figs. 30–34, we observed that the Bejan number increases along the centreline region and at the walls with an increase in the parameter values of β, *Ec*, λ, *Nt*, and *A*. This implies that a decrease in nanofluid viscosity coupled with a combined increase in viscous heating, thermophoresis, and pressure gradient may enhance the dominant effect of heat and mass transfer irreversibilities along the centreline region and at the walls. As the Brownian motion parameter *Nb* increases, the dominant effects of fluid friction irreversibility are enhanced both along the channel centreline region and at the walls, as illustrated in Fig. 35.

6. Conclusions

The flow structure, heat transfer and entropy generation in an unsteady channel flow of a variable viscosity water-based nanofluid with convective heat exchange with the ambient atmosphere at the walls are numerically investigated. Using a semi-discretisation finite-difference method together with a Runge–Kutta–Fehlberg integration scheme, the model nonlinear initial boundary value problem is tackled. Some of the results obtained can be summarised as follows:

- the nanofluid's velocity and temperature profiles increase with increasing t, β, *Ec*, but decreases with increasing *Bi*;
- nanoparticle concentration increases along the centreline region and decreases near the walls, with an increase in t, β, *Ec*, *Nt*. However, an increase in *Bi* or *Nb* causes a decrease in nanoparticle concentration along the centreline region, whereas the concentration increases near the walls;
- the skin friction increases with t, β, *Ec*, *Nt* and *A*, but decreases with *Ec* and *Nt*. The Nusselt number increases with t, *Ec*, *Bi* and β;

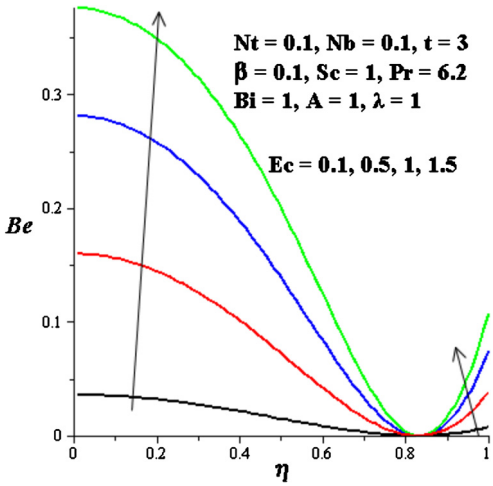

Fig. 31. (Colour online.) Bejan number with increasing *Ec*.

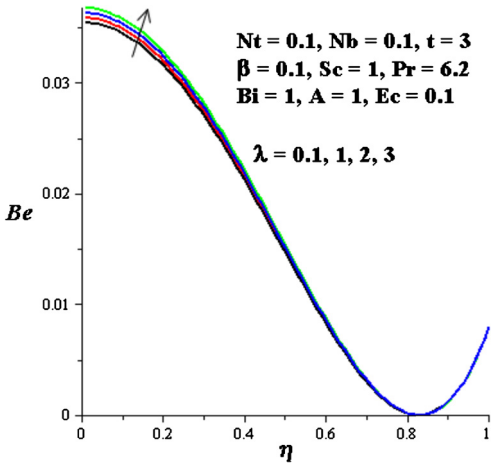

Fig. 32. (Colour online.) Bejan number with increasing λ.

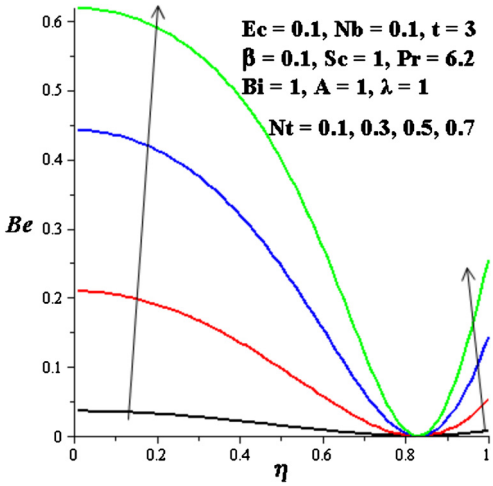

Fig. 33. (Colour online.) Bejan number with increasing *Nt*.

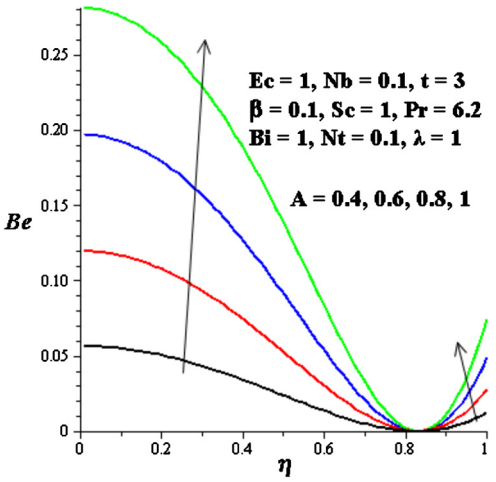

Fig. 34. (Colour online.) Bejan number with increasing *A*.

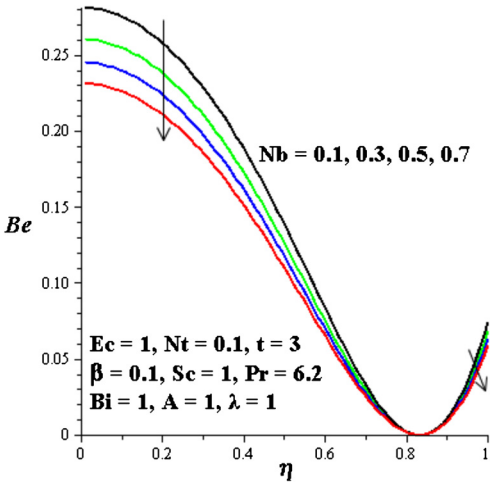

Fig. 35. (Colour online.) Bejan number with increasing *Nb*.

- the entropy generation rate generally increases with t, Ec, β, A, Nt. A Bi increase increases entropy generation at the walls, but decreases entropy generation within the channel;
- the Bejan number within the centreline region and at the walls increases with t, Ec, β, A, Nt and λ; consequently, the dominant effects of heat transfer and nanoparticle mass transfer irreversibilities increase.

Finally, from the above, we conclude that with careful combination of parameter values, the entropy production within the channel flow of a variable-viscosity water-based nanofluid in the presence of convective cooling can be minimised.

References

[1] S.U.S. Choi, Enhancing thermal conductivity of fluids with nanoparticles, in: Proc. ASME Int. Mech. Eng. Congress and Exposition, ASME, San Francisco, USA, 1995, pp. 99–105, FED 231/MD 66.
[2] S.U.S. Choi, Z.G. Zhang, W. Yu, F.E. Lockwood, E.A. Grulke, Anomalously thermal conductivity enhancement in nanotube suspensions, Appl. Phys. Lett. 79 (2) (2001) 2252–2254.
[3] E. Abu-Nada, Application of nanofluids for heat transfer enhancement of separated flows encountered in a backward facing step, Int. J. Heat Fluid Flow 29 (2008) 242–249.
[4] O.D. Makinde, A. Aziz, Boundary layer flow of a nanofluid past a stretching sheet with a convective boundary condition, Int. J. Therm. Sci. 50 (2011) 1326–1332.
[5] O.D. Makinde, Effects of viscous dissipation and Newtonian heating on boundary layer flow of nanofluids over a flat plate, Int. J. Numer. Methods Heat Fluid Flow 23 (8) (2013) 1291–1303.
[6] W.N. Mutuku-Njane, O.D. Makinde, Combined effect of buoyancy force and Navier slip on MHD flow of a nanofluid over a convectively heated vertical porous plate, Sci. World J. 2013 (2013) 725643 (8 pp.).
[7] M. Olanrewaju, O.D. Makinde, On boundary layer stagnation point flow of a nanofluid over a permeable flat surface with Newtonian heating, Chem. Eng. Commun. 200 (6) (2013) 836–852.

[8] O.D. Makinde, Analysis of Sakiadis flow of nanofluids with viscous dissipation and Newtonian heating, Appl. Math. Mech. 33 (12) (2012) 1545–1554.
[9] T.G. Motsumi, O.D. Makinde, Effects of thermal radiation and viscous dissipation on boundary layer flow of nanofluids over a permeable moving flat plate, Phys. Scr. 86 (2012) 045003 (8 pp.).
[10] K.S. Hwang, J.-H. Lee, S.P. Jang, Buoyancy-driven heat transfer of water-based Al_2O_3 nanofluids in a rectangular cavity, Int. J. Heat Mass Transf. 50 (2007) 4003–4010.
[11] D.A. Nield, A.V. Kuznetsov, The Cheng–Minkowycz problem for natural convective boundary-layer flow in a porous medium saturated by a nanofluid, Int. J. Heat Mass Transf. 52 (2009) 5792–5795.
[12] H.F. Oztop, E. Abu-Nada, Numerical study of natural convection in partially heated rectangular enclosures filled with nanofluids, Int. J. Heat Fluid Flow 29 (2008) 1326–1336.
[13] W. Ibrahim, O.D. Makinde, The effect of double stratification on boundary-layer flow and heat transfer of nanofluid over a vertical plate, Comput. Fluids 86 (2013) 433–441.
[14] O.D. Makinde, W.A. Khan, Z.H. Khan, Buoyancy effects on MHD stagnation point flow and heat transfer of a nanofluid past a convectively heated stretching/shrinking sheet, Int. J. Heat Mass Transf. 62 (2013) 526–533.
[15] O.D. Makinde, Computational modelling of nanofluids flow over a convectively heated unsteady stretching sheet, Curr. Nanosci. 9 (2013) 673–678.
[16] X.Q. Wang, A.S. Mujumdar, Heat transfer characteristics of nanofluids: a review, Int. J. Therm. Sci. 46 (2007) 1–19.
[17] J. Buongiorno, Convective transport in nanofluids, J. Heat Transf. 128 (2006) 240–250.
[18] W.N. Mutuku-Njane, O.D. Makinde, MHD nanofluid flow over a permeable vertical plate with convective heating, J. Comput. Theor. Nanosci. 11 (3) (2014) 667–675.
[19] R.K. Tiwari, M.K. Das, Heat transfer augmentation in a two-sided lid-driven differentially heated square cavity utilizing nanofluids, Int. J. Heat Mass Transf. 50 (2007) 2002–2018.
[20] A. Bejan, Second-law analysis in heat transfer and thermal design, Adv. Heat Transf. 15 (1982) 1–58.
[21] A. Bejan, Entropy Generation Minimization, CRC Press, Boca Raton, FL, USA, 1996.
[22] L.C. Woods, Thermodynamics of Fluid Systems, Oxford University Press, Oxford, UK, 1975.
[23] U. Narusawa, The second-law analysis of mixed convection in rectangular ducts, Heat Mass Transf. 37 (1998) 197–203.
[24] A.Z. Sahin, Second law analysis of laminar viscous flow through a duct subjected to constant wall temperature, J. Heat Transf. 120 (1998) 76–83.
[25] O.D. Makinde, A. Aziz, Second law analysis for a variable viscosity plane Poiseuille flow with asymmetric convective cooling, Comput. Math. Appl. 60 (2010) 3012–3019.
[26] O.D. Makinde, O.A. Beg, On inherent irreversibility in a reactive hydromagnetic channel flow, J. Therm. Sci. 19 (1) (2010) 72–79.
[27] O.D. Makinde, W.A. Khan, A. Aziz, On inherent irreversibility in Sakiadis flow of nanofluids, Int. J. Exergy 13 (2) (2013) 159–174.
[28] T.Y. Na, Computational Methods in Engineering Boundary Value Problems, Academic Press, New York, 1979.